THE JOURNAL OF PHYSICAL CHEMISTRY C
A JOURNAL OF THE AMERICAN CHEMICAL SOCIETY

pubs.acs.org/JPCC
Article

BA_2SnI_4 as a Promising 2D Ruddlesden–Popper Perovskite for Optoelectronic Applications

J. F. Dalmedico, D. N. Silveira, Carlos Maciel O. Bastos, C. R. C Rêgo, Alexandre Cavalheiro Dias, D. Guedes-Sobrinho, and Maurício J. Piotrowski*

Cite This: J. Phys. Chem. C 2025, 129, 9646–9655
Read Online

ACCESS | Metrics & More | Article Recommendations | Supporting Information

ABSTRACT: Lead-free two-dimensional (2D) hybrid metal halide perovskites (MHPs) emerge as promising eco-friendly alternatives to lead-based counterparts, offering excellent thermodynamic stability and environmental compatibility despite lower solar harvesting efficiency. Nonetheless, the dearth of research on tin-based MHPs illustrates the difficulties in their optoelectronic characterization. Herein, we present a computational protocol that integrates *ab initio* and semiempirical approaches to investigate the electronic, optical, and excitonic properties of the scarcely explored BA_2SnI_4, where BA represents butylammonium. We apply a cost-effective computational framework that combines a maximally localized Wannier function tight-binding (MLWF-TB) method for electronic states with the Bethe–Salpeter equation (BSE) for excitonic properties. To improve the accuracy of the electronic band gap, we employ a relativistic quasi-particle correction (DFT-1/2) within the density functional theory (DFT) framework, which also includes van der Waals corrections and spin–orbit coupling effects. Our findings reveal that replacing Pb with Sn weakens exciton binding, leading to lower exciton binding energies and improved charge extraction efficiency. These results indicate a band gap of 2.0 eV, an exciton ground state energy of 1.85 eV, and an exciton binding energy of 150 meV. The BSE calculations also predict a redshift in absorption, extending the spectral response further into the visible range, compared to the independent particle approximation (IPA). 2D RP BA_2SnI_4 perovskite is a promising photovoltaic material since even in ultrathin films smaller than 0.25 μm, this material can achieve PCE values near 25%, close to the Shockley–Queisser limit. Although Sn-based 2D MHPs present advantageous features, more work is required to resolve manufacturing issues and enhance performance stability.

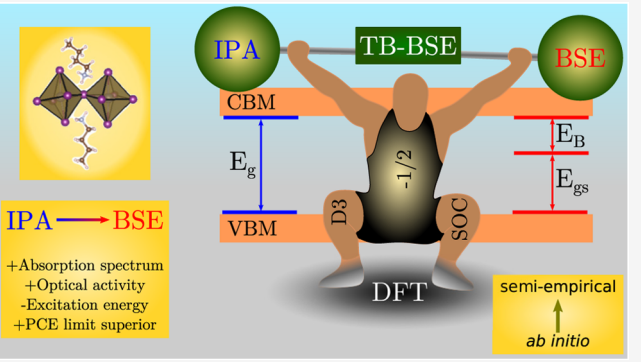

1. INTRODUCTION

Two-dimensional (2D) hybrid metal halide perovskites (MHPs) have been found promising as low-dimensional materials for commercially viable next-generation photovoltaic solar cells because of their improved optoelectronic characteristics and enhanced stability when compared to their three-dimensional (3D) counterparts.[1−3] 2D-MHPs are advantageous due to combining the best features of 3D and 2D semiconductors,[3,4] having promising optoelectronic properties, including efficient light absorption, increased defect tolerance, and tunable excitonic effects.[5] Notwithstanding this favorable situation, there are still many challenges awaiting resolution to unveil their structural features and how the external perturbations affect synthesized films, particularly intending to raise their power conversion efficiency (PCE).[4]

Lead-based MHPs have been extensively investigated concerning perovskite solar cell (PSC) applications, with significant advances toward commercialization despite their toxicity and stability problems.[4,6−10] The PCE of lead-based MHPs reaches 25%[11] for 3D and 17%[12] for 2D, matching Si-based photovoltaic devices (26%[13,14]) and presenting a promising performance when mixing 2D/3D heterostructures (23%[15]) and/or tandem Pb–Sn (>29%[16]). However, the lead toxicity and environmental impacts call for the substitution by metals such as tin,[1,17,18] which exhibit analogous optoelectronic properties.[19,20]

In this line, Ruddlesden–Popper (RP) MHPs with butylammonium spacer (BA = $CH_3(CH_2)_3NH_3^+$) achieved an efficiency of ∼17%[12,21,22] with variations relative to the architecture of choice. Conversely, tin-based 2D RP MHPs containing BA exhibited a significantly lower PCE of ∼2.5%.[23] This alarming efficiency reduction is likely due to Sn oxidation,[24] precursor impurities,[25] noncontrolled crystalliza-

Received: March 13, 2025
Revised: May 13, 2025
Accepted: May 14, 2025
Published: May 18, 2025

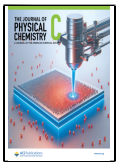

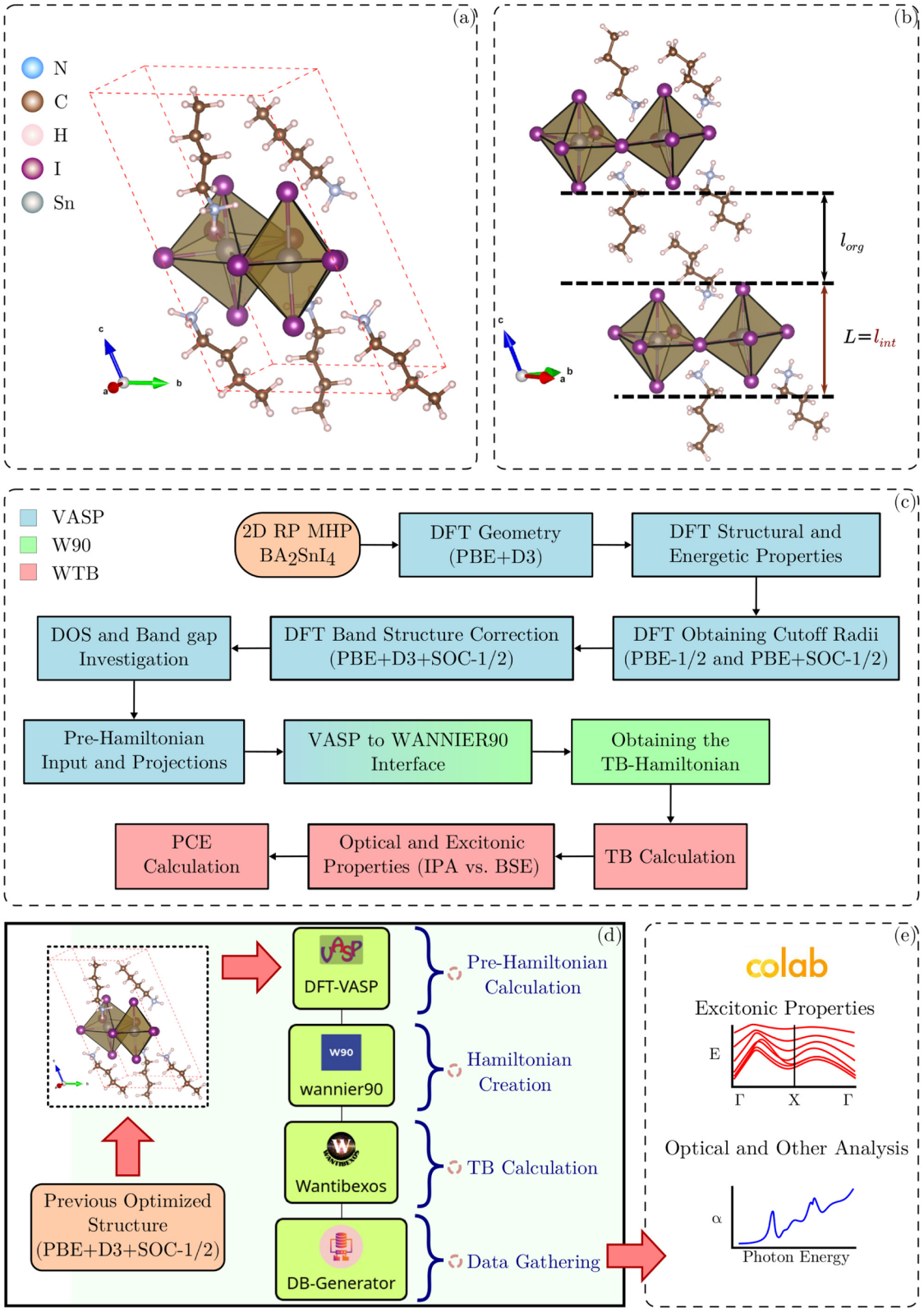

Figure 1. 2D RP MHP BA_2SnI_4 supercell from (a) isometric and (b) lateral perspectives. The composition is highlighted by the organic (l_{org}) and inorganic ($L = l_{int}$) layers. Additionally, (c) presents the flowchart of calculations, from *ab initio* to semiempirical approaches. Panel (d) illustrates the SimStack workflow employed for calculating the geometrical and electrical properties of the BA_2SnI_4 supercell using the WaNos: DFT-VASP, Wannier90, Wantibexos, and DB-Generator. Panel (e) shows the graphics of photonics and optical properties analyzed in a Google Colab, which retrieves data directly from the DB-Generator WaNo.

tion,[26] and/or low film quality,[27,28] directly affecting the optoelectronic properties. Sn is a promising alternative to Pb and needs further investigation into better architecture to start the full potential of Sn-based PSCs.[29,30]

https://doi.org/10.1021/acs.jpcc.5c01707
J. Phys. Chem. C 2025, 129, 9646−9655

Optoelectronic behavior in 2D perovskites is highly tunable by chemical engineering of organic and inorganic layers,[31] directly controlling key parameters like energy band gap, light absorption, and exciton binding energy.[32] These impacts come from dielectric and quantum confinement, which dictate the excitonic behavior[33,34] and the charge dissociation for transportation purposes.[35] Electronic and optical properties are also greatly influenced by structural factors, such as local phase inhomogeneities, octahedral distortions, layer thickness, organic−inorganic interactions, and dielectric environment, all that cause symmetry breaking and alter the dielectric landscape;[36,37] thus altering film crystallization, spintronics, and optoelectronic properties.[4] Hence, understanding film engineering and optoelectronic behavior is critical to improving the production and commercialization of solar cells. Except for recent research,[38−40] the excitonic properties and another optoelectronic feature of 2D-MHPs are still poorly explored and need further investigation.

Accurate theoretical modeling is crucial as excitonic effects lie at the heart of the definition of the optical band gap and linear optical response of 2D perovskites. However, due to the many-body problem, electron−hole (e−h) interactions present significant computational challenges, especially in 2D systems where the quantum confinement in the vacuum direction enhances these quasiparticle effects. Pure *ab initio* + Bethe−Salpeter equation (BSE)[41−43] calculations of excitonic properties in complex systems, such as RP MHPs,[34,44−46] are typically impossible due to prohibitive computational costs, to address this challenge, several methods have been employed, including Wannier-Mott exciton descriptions, which depends of electron and hole effective masses, and the combination of maximally localized Wannier function tight binding approach (MLWF-TB) + BSE approaches.[40,47]

Continuing in this direction, in a recent study,[48] we examined the structural stability and electronic properties of 2D RP $BA_2MA_{n-1}B_nX_{3n+1}$ perovskites, with B = Ge or Sn and X = Br or I, for n = 1−5 layers, and 3D bulk $(MA)BX_3$ systems. We noted a pronounced influence of atoms with smaller ionic radii, which induced anisotropic internal and external distortions in the organic and inorganic lattices despite stabilizing the organic spacers. Thus, that these 2D RP MHPs possess structural stability, adjustable band gaps, and distinct electronic properties has been ascertained, making them solid prospects for optoelectronic devices, with special interest for tin-based compounds, namely on BA_2SnI_4 for n = 1, which exhibit better stability and less distortion compared to their Br-based counterparts and bulk. These findings suggest that BA_2SnI_4 is an excellent candidate for further exploration of excitonic effects in lead-free perovskites.

Given the key function of excitons in characterizing optical features, this study focuses on quantifying the exciton binding energy, examining the linear optical response through the absorption spectrum, and investigating the charge carrier dynamic in BA_2SnI_4. This is crucial to achieve optimal charge separation and 2D perovskite-based optoelectronic devices. Our proposal for the system adheres to the lead-free perovskite trend since Sn-based counterparts are more environmentally friendly (eco-friendly) than Pb-based systems. Furthermore, we employ a cost-efficient computation that incorporates relativistic quasi-particle correction (DFT-1/2), van der Waals (vdW) corrections, spin−orbit coupling (SOC), and maximally localized Wannier function tight-binding (MLWF-TB) methods and, subsequently, computations involving BSE. This hybrid methodology provides accurate excitonic property predictions with reduced computational costs and offers insightful information for rational optimization of lead-free perovskites for application in solar energy.

2. METHODOLOGY

2.1. *Ab Initio* Calculations. Our structural relaxation calculations are based on spin-polarized DFT,[49,50] considering the standard semilocal Perdew−Burke−Ernzerhof (PBE) functional[51,52] for the exchange and correlation functional, as implemented in the vienna *ab initio* simulation package (VASP).[53−55] As it is known that DFT-PBE calculations underestimate the band gap[56−58] and do not describe dispersion forces adequately, we employed the quasi-particle method DFT-1/2[59,60] and vdW-D3[61−63] corrections, respectively, since they are well-tested with promising results in previous studies.[8,10,64] Similarly, in contrast to the scalar relativistic treatment offered by VASP default calculations for the valence electrons, we have included the spin−orbit coupling (SOC)[65,66] effects in the valence states, for a correct description of orbital relativistic effects, due to the dense cores of the inorganic layer. Given that 2D RP MHPs are complex atomic structures, a robust approach set is needed to describe their physical properties correctly. Therefore, we have considered a well-established protocol labeled as DFT-PBE +D3+SOC-1/2.[10,48] More technical details on the DFT-1/2 quasi-particle correction method, including the determination of the cutoff radius function (CUT parameter optimization), can be found in our previous publication.[48]

To solve the Kohn−Sham (KS) equations, we have considered the projector augmented wave (PAW) method,[67] as implemented in VASP, with KS orbitals expanded in plane-waves up to a specified cutoff energy of 500 eV, which exceeds the VASP recommended values (ENMAX). The Brillouin zone (BZ) integration was sampled with a 4 × 4 × 3 **k**-point mesh. For the density of states and band structure calculations, the **k**-point mesh was increased by an additional 25%. Equilibrium geometries were obtained by minimizing the atomic forces on every atom until 0.01 eV/Å, while a total energy convergence of 10^{-6} eV was adopted for electronic self-consistency.

An orthorhombic supercell of size 2 × 1 × 1 was employed for our 2D RP MHP BA_2SnI_4 calculation for a better description of the interaction between the organic parts, with the inorganic layer (SnI) along *xy* plane and organic layer (BA) along the *z*-axis as shown in Figure 1(a). To clarify the separation among periodic systems along the *z*-axis, panel (b) illustrates the organic layer size (l_{org}) between two inorganic layers, each with a thickness of l_{int}. The organic (spacer) layer is composed of hydrophobic butylammonium (BA) molecules, while the inorganic layer is populated by SnI-based framework. This configuration results in a supercell containing 78 atoms, with 16 C, 4 N, 48 H, 2 Sn, and 8 I atoms. Finally, panel (c) shows the complete calculations workflow for all calculations performed, while additional computational details are provided in the Supporting Information.

2.2. Wannierization. We construct a TB Hamiltonian (MLWF-TB) based on MLWFs using Wannier90.[68] This procedure is carried out as a postprocessing step after the *ab initio* calculation, where the KS Hamiltonian is projected onto the MLWF basis. For the Wannierization process, we consider s and p orbital projections for Sn and I, and only p orbital projections for C and N, while importing calculation data from a previous VASP run. All projections include spinors.

https://doi.org/10.1021/acs.jpcc.5c01707
J. Phys. Chem. C 2025, 129, 9646−9655

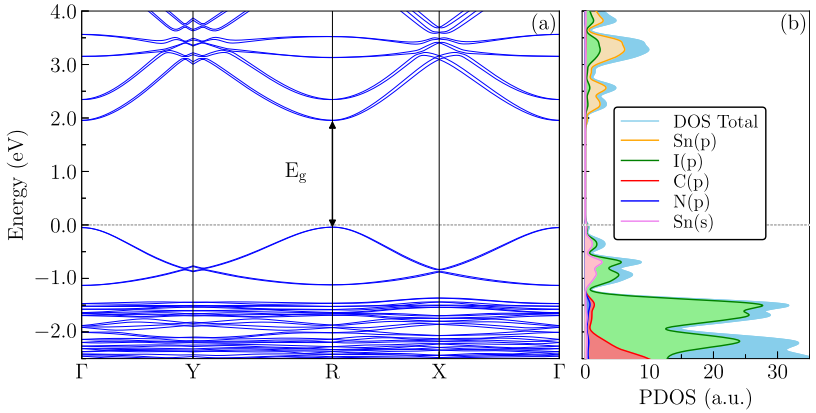

Figure 2. Electronic structure of the 2D RP MHP BA_2SnI_4 calculated using the DFT-PBE+D3+SOC-1/2 protocol, (a) the band structure and (b) the projected density of states. The Fermi level is set to 0 eV.

2.3. Semiempirical Calculations for the Optical Properties. We have used the WanTiBEXOS package[47] to predict the optical and excitonic properties *via* BSE[69] with the Tamm−Dancoff approximation (TDA), incorporating excitonic effects described by the Bare Coulomb Potential (V3D), and also performing PCE calculations. The electron and hole single−particle states were described for the MLWF-TB Hamiltonian, obtained from DFT-PBE+D3+SOC-1/2 calculations. The BSE was solved using a **k**-points mesh of 11 × 11 × 6 which corresponds to a **k**-points density of 90 $Å^{-1}$ considering the 6 highest valence bands and the 2 lowest conduction bands, which is sufficient for a description of the absorption coefficient in the solar emission spectrum range (0.5 to 4.0 eV).[70] We applied smearing of 0.05 eV to the dielectric functions at both BSE and IPA levels to ensure accurate results. The prediction of the optical properties is based on the real and imaginary parts of the dielectric tensor initially calculated in the independent particle approximation (IPA). We derive the refractive index and the extinction coefficient from the dielectric function parts, whose interplay determines the reflectivity. The absorption coefficient is obtained from the dielectric function as well.

2.4. Scientific Workflow Using SimStack Framework. The *ab initio* and semiempirical calculations were carried out using the SimStack framework,[71] through Workflow Active Nodes (WaNos), and it enabled the implementation of the calculation flow illustrated in Figure 1(c). The generated data, input files, and additional information on how to run the workflow are readily accessible in our GitHub repository. Including the specific data on the optical transition dipole moments, containing the linear polarization-resolved transition dipole matrix elements for the *xx*, *yy*, *zz*, *xy*, *xz*, and *yz* tensor components. The scientific workflow principle saves time for large, complex, and demanding systems, providing a more reliable approach to managing a large complex of calculations while reproducibility and transferability are ensured.[72−78] This means reducing the time consumed during the presubmission and postexecution phases. Below, we focus on the workflow dynamics and the design of choice to predict the physical properties of our 2D RP MHP system.

The first half of our protocol relies on the DFT-VASP WaNo for structure optimization, stress tensor, and energetic and electronic structure calculations. DOS, band structure, band gap, structural parameter, and energetic analysis came from this phase alone. This WaNo facilitates DFT calculations *via* VASP[53−55] software by automatically handling input files, including the structure depicted in Figure 1a, and efficiently manages standard structure-electronic optimization protocols with simplicity and efficiency. Additionally, we can manipulate this WaNo into standard calculations or directly import input files, simplifying and accelerating the presubmission and allowing easy control of memory usage, node relocation, and thread optimization.

The Figure 1d shows a SimStack workflow employed for the passage *ab initio* to semiempirical scopes. We apply a set of WaNos to generate a TB-Hamiltonian, starting with a DFT-VASP and taking advantage of the VASP to wannier90 interface to generate Wannier input files. This feature completes the Wannierization inputs that are ready to use in the next phase, excluding the need for an intermediate presubmission phase. Next, we Wannierize the previously optimized structure (DFT-PBE+D3+SOC-1/2 protocol) using the wannier90 WaNo, creating an MLWF-TB Hamiltonian. For optical and excitonic prediction, we introduce this Hamiltonian into the Wantibexos WaNo. This step preprocesses the Hamiltonian to a WanTiBEXOS[47] format and could fragment the processes between excitonic, optical, and electronic focus calculation or predict all at once. Finally, the auxiliary DB-Generator WaNo organizes the generated data as a.yml format file, making key information easily accessible and exportable for postprocessing using Google Colab or cloud Jupyter Notebook, as highlighted by Figure 1e.

3. RESULTS AND DISCUSSION

3.1. Energetic and Structural Properties. Our studied system was derived from the 2D RP MHP $A'_2A_{n-1}B_n X_{3n+1}$ family, setting $n = 1$, with metal B = Sn, halogen X = I, organic spacer A′ = BA. Since $n = 1$, there is no organic cation A. Our 2D RP MHP BA_2SnI_4 system is thermodynamically stable, mainly due to the majority contribution from the organic layers, presenting a higher enthalpy of formation (−6.28 eV) than the 2D systems with $n > 1$ layers than the 3D system ($n = \infty$). Structurally, our system adopts an orthorhombic crystal structure with equilibrium lattice parameters $a_0 = 8.18$ Å, $b_0 = 8.69$ Å, and $c_0 = 15.47$ Å, and equilibrium angles: $\alpha = 113.6^o$, $\beta = 92.8^o$, and $\gamma = 90.3^o$. The layer thicknesses are $l_{org} = 6.98$ Å and $L = l_{int} = 6.37$ Å. Furthermore, the inorganic structure (SnI_4) maintains centrosymmetry, with the spacer (BA) penetrating −0.75 Å (0.59 Å) at the upper (lower) interface. This penetration influences the dipolar effects of the spacer

https://doi.org/10.1021/acs.jpcc.5c01707
J. Phys. Chem. C 2025, 129, 9646−9655

BA, reducing the octahedral distortions. The remaining distortions include: (i) smaller distortions in metal−halogen bond lengths and (ii) lower variations in bond angles compared to similar family systems with $n > 1$ or $n = \infty$.[48] More details on energetic and structural properties are provided in the Supporting Information, showing excellent agreement with our previous work.[48]

3.2. Electronic Properties. To understand the electronic structure of our 2D RP MHP BA_2SnI_4 system, we calculated the band structure and the orbital-projected density of states as shown in Figure 2a,b, respectively, while the values for the band gap (E_g), exciton ground-state (E_{gs}), and exciton binding energy (E_B) are provided in Table 1. More details about the band structure, including the **k**-path are given in Supporting Information. From the band structure in panel (a), a semiconductor behavior is evident, characterized by a direct bandgap present at the *R* symmetric point in BZ. Although one might initially consider the band edge to be localized at the Γ point, this is not the case, as the possible gap at Γ is only 0.4% wider than at *R*. Therefore, to refine our predictions, we considered relativistic SOC effects and the quasi-particle correction (DFT-1/2 method). Compared to computations without this adjustment, the SOC inclusion produced a 7.5% band gap reduction. In contrast, the DFT-1/2 technique produced a notable 43% band gap increase, indicating its influence on the electronic structure.

Table 1. Electronic and Optical Properties of the 2D RP BA_2SnI_4 Perovskite: Band Gaps (E_g), Exciton Ground State Energies (E_{gs}), and Exciton Binding Energies (E_B)[a]

E_g (eV)	E_{gs} (eV)	E_B (meV)	refs
2.00	1.85	150	this work
2.35	2.18	170 ± 20	Hansen et al.[81]
1.53	–	268	Chen et al.[38]
2.04	–	286	Ma et al.[82]
1.45	–	267	Ma et al.[83]

[a]Additionally, theoretical and experimental values compiled from the literature are compared

Therefore, through our full DFT-PBE+D3+SOC-1/2 protocol, we have predicted E_g of 2.0 eV, as shown in Figure 2a and presented in Table 1. This value is in good agreement with experimental results reported in the literature: 1.98 eV,[6] obtained *via* photoluminescence (PL) spectroscopy using an argon ion laser; and 2.35 eV,[79] measured through low-temperature electro-absorption spectroscopy. The band gap obtained for BA_2SnI_4 is lower than the value of 2.54 eV reported for PbI-based 2D RP MHPs,[34] measured by optical spectroscopy.

A detailed analysis of the electronic structure close to the Fermi level is illustrated in the DOS plot in Figure 2b. Our results for Sn-based MHPs show that the valence band maximum (VBM) is predominantly composed of iodine p orbitals and tin s orbital, while tin p orbitals dominate the conduction band minimum (CBM); which is in opposition to Pb-based MHPs, where only Pb dominates the valence band. Interestingly, this deviation contrasts with previous theoretical results of electronic similarity between Sn-and Pb-based MHPs,[80] suggesting that iodine p orbitals play a more significant role in defining the valence band features.

Moreover, this change in the valence band composition results in implications for E_B. While the direct band gap is equal to 2.0 eV, our calculations yield an exciton ground state (E_{gs}) of 1.85 eV, which implies an exciton binding energy (E_B) of 150 meV. Consequently, the dominant contribution from the iodine orbitals modifies the electronic structure, distinguishing Sn-based MHPs from their Pb-based counterparts. These findings highlight the fundamental differences in the electronic properties of Sn-and Pb-based 2D RP MHPs and their potential impact on optoelectronic applications, putting Sn-based systems in the running once and for all.

WanTiBEXOS predicts hole (electron) effective masses m_h^* (m_e^*) of 4.61 (0.20), 1.13 (0.82), and 8.28 (116.34) along the *xx*, *yy*, and *zz* tensor components, respectively. These values reveal significantly higher electron mobility compared to hole mobility, especially along the in-plane directions. However, the *zz*-component indicates a strong suppression of carrier mobility perpendicular to the inorganic layers, likely due to the presence of organic spacers acting as transport barriers. The combination of light in-plane effective masses and a low exciton binding energy supports the potential of this material as an efficient photoabsorber in optoelectronic and photovoltaic applications.[84]

3.3. Excitonic and Optical Properties. The excitonic band structure of 2D RP BA_2SnI_4 perovskite, obtained from MLWF-TB+BSE approach, is shown in Figure 3. We found an exciton ground state energy of 1.85 eV, with an exciton binding energy of 150 meV, calculated by $E_g - E_{gs}$. These findings are in agreement with other studies on 2D MHPs (see Table 1, which compares our DFT-1/2+TB-BSE results with other theoretical and experimental studies),[2,4] and confirms that BA_2SnI_4 exhibits a direct exciton transition; however, at *R* point we have an indirect excitonic state with very closer energy, which suggests the possibility of phonon-assisted optical transitions for light excitations with similar frequencies. As a result of the linear optical response, all exciton transitions below the electronic band gap appear as bright excitonic states, enabling direct spin transitions (see Supporting Information for the spin-polarized band structure).

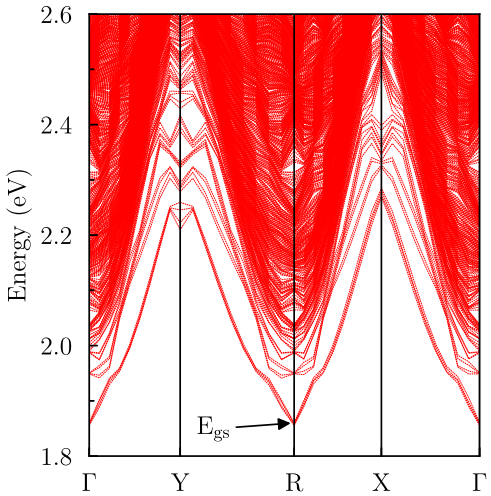

Figure 3. Exciton band structure of the 2D RP BA_2SnI_4 perovskite, obtained using MLWF-TB+BSE with a DFT-PBE+D3+SOC-1/2-based parametrization.

Hansen et al.[81] reported a low-temperature electroabsorption spectroscopy measurement yielding an E_g of 2.35 eV, followed by an E_{gs} of 2.18 eV, and an E_B of 170 meV (±20 meV). However, using low-temperature time-resolved photo-

https://doi.org/10.1021/acs.jpcc.5c01707
J. Phys. Chem. C 2025, 129, 9646−9655

luminescence combined with an Arrhenius model fit of PL intensity, a second analysis yielded an E_{gs} of 1.99 eV and an E_B of 48 meV (±40 meV). From a theoretical perspective, Chen et al.[38] employed HSE06 calculations and reported an E_g of 1.53 eV and a E_B of 268 meV based on the Wannier−Mott exciton model. Similarly, Ma et al.[82] obtained an E_B of 286 meV, but an E_g of 2.04 eV using the PBE0+SOC functional-protocol. Meanwhile, Ma et al.[83] incorporated relativistic corrections into HSE06 (HSE06+SOC), obtaining an E_g of 1.45 eV and an E_B of 267 meV.

Compared to the respective Pb-based system, our Sn-based perovskite presented a band gap reduction of 26% (2.5 eV[34]), a E_{gs} reduction of 23% (~2.4 eV[9]), and a E_B reduction of 68% (467 meV[34]). A lower E_B indicates a weaker electron−hole interaction favors exciton dissociation and increases charge extraction efficiency, a desired property for solar cell applications. Those findings make Sn-based 2D RP MHPs promising materials for optoelectronic applications.

Figure 4(a) illustrates the absorption coefficients (α_i) at IPA and BSE levels, both within the visible light at absorption spectrum (1.6−3.2 eV). The in-plane BSE absorption tensors exhibit a similar trend for the IPA approach due to the noncentrosymmetric behavior,[38] followed by peaks at 3.0 eV and weak response at out-of-plane (z-axis direction) absorption. The presence of flat bands (see the Supporting Information for more details on band structure) explains the z tensor absorption and anisotropy. The α_i behavior aligns with literature results for Sn-based 2D RP MHPs computed using hybrid functionals.[38,85] However, our band edge onset (2.0 eV) is higher than previously reported absorption energies (1.53[38] and 1.84 eV[85]).

We observed a stronger optical response in the x and y directions, with reduced absorption for z-incidence, which reflects the influence of the organic spacer and dielectric confinement effects in 2D MHPs.[34,86−90] This optical anisotropy demonstrates that the influence of the organic spacer results in reduced charge carrier efficiency at incidence normal to the organic layer. The electronic states are localized in their respective layers, having a negligible overlap between adjacent layers, *i.e.*, we practically do not have interlayer electron−hole transitions. Thus, according to our results, perovskite thin films should be orientated with the inorganic layers perpendicular to the substrate to optimize charge carrier extraction in solar cell applications.[2]

The BSE approach predicted a red-shift in the absorption spectrum and improved photon absorption efficiency. In comparison to the reported ~2.4 eV for PbI-based MHPs,[9] our SnI-based MHP reached an absorption peak at 1.85 eV; representing a −23% deviation. This absorption at lower energies than E_g enhanced the absorption coefficient at 1.75−2.87 eV light spectrum interval. Therefore, Sn-based MHPs have the potential for solar cell applications.

Despite following a similar trend, the refractive index shown in Figure 4b indicates that photons experience more significant slowing at lower energies. This behavior change for excitation energies higher than 3.0 eV where the refractive index begins to diminish, being the same region where the reflective enhances, achieving a maximum value around 22.5% at IPA and 17.5% at BSE level, as shown in Figure 4c.

Our results suggest that lower-dimensional MHPs exhibit higher reflection peaks at transition states, with negligible reflection in the z-direction. In general, the BSE approach enhances the description of the electronic transitions and

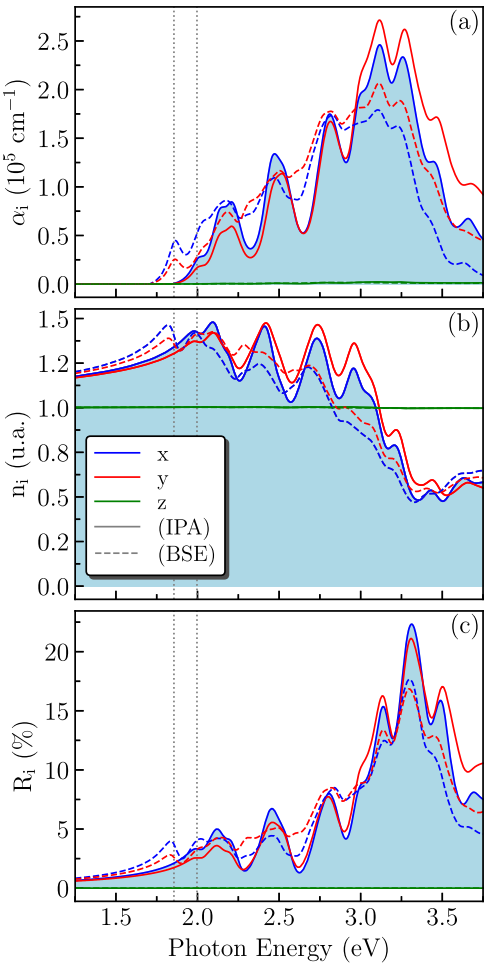

Figure 4. (a) Absorption coefficient (α_i), (b) refractive index (n_i), and (c) reflectivity coefficient (R_i) within the visible spectrum for in-plane (x−y) and out-of-plane (z) incidence directions for the 2D RP BA_2SnI_4 perovskite. All results are presented for both the IPA (solid curves) and BSE (dashed curves) approaches and considers incident light polarizations at x (blue curves), y (red curves), and z (green curves) directions. Vertical dashed gray lines indicate the excitation energy (E_{gs}) and band gap energy (E_g), which define the exciton binding energy (E_B). Further details on the variation of these properties for out-of-plane incidence are provided in the Supporting Information.

absorption over a broader energy range (1.85−2.75 eV), except for reduced excitation probabilities along the z-axis. The observed redshift in excitation energies highlights the strong impact of electron−hole interactions within the system.

3.4. PCE Prediction. The difference in PCE in Figure 5 highlights the solar harvesting efficiency enhancement due to excitonic effects. The bright exciton at 1.85 eV enabled a 13% higher PCE (25.5%) than the standard IPA result (22.5%). However, Sn-based MHPs with such high PCE values have yet to be realized experimentally. According to some studies,[84,91,92] the reduction in the MHP dimensionality caused by the organic layer presence,[31] is responsible for the efficiency drop. On the other hand, other works suggest that the efficiency loss is favored by the inhibition of carrier transport and nonradiative recombination brought on by highly localized and strongly bound excitons.[93,94]

An alternative to address these limitations lies in the mixed 2D/3D structures proposal.[95,96] However, it should be noted

https://doi.org/10.1021/acs.jpcc.5c01707
J. Phys. Chem. C 2025, 129, 9646−9655

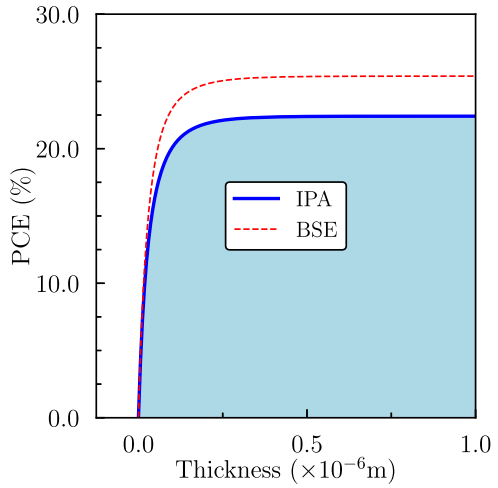

Figure 5. PCE calculated through SLME for the 2D RP BA_2SnI_4 perovskite using both the IPA and BSE approaches as a function of MHP thickness.

that long-term stability is more important for commercialization than getting a PCE value around the maximum achieved for a single photoabsorber predicted at Shockley–Queisser limit (SQ limit).[97] While Sn-based perovskite solar cells may experience oxidation problems[24] and poor film quality,[27,28,98] studies suggest that PCEs beyond 19% may be achieved by optimizing crystallization[26] and/or implementing advanced materials engineering strategies.[27]

4. CONCLUSIONS

We have investigated the electronic, optical, and excitonic properties of the 2D RP BA_2SnI_4 (BA = butylammonium) perovskite using a robust workflow combining *ab initio* and semiempirical methods, which included DFT-PBE+D3+SOC-1/2 and MLWF-TB (BSE and IPA frameworks) calculation protocols, respectively. Based on the SimStack framework, our workflow established robust, automated protocols that consistently yielded reproducible results, integrating DFT and MLWF-TB methods. We minimized manual intervention, ensuring standardized and efficient processes for advanced property predictions. By using the workflow we were able to identify some advantages of Sn-based MHPs over Pb-based counterparts, *i.e.*, BA_2SnI_4 exhibits a narrower band gap (2.0 eV) and lower exciton ground state energy (1.85 eV), suggesting enhanced exciton dissociation (exciton binding energy of 150 meV) and improved charge extraction efficiency. Furthermore, we found that the quasi-particle method (DFT-1/2) is a reliable correction for the electronic structure throughout our computational routine (correcting the band gap by 43% concerning the standard DFT-PBE protocol), from the BSE approach, we obtained more accurate optical predictions (than IPA), revealing a broader excitation spectrum and a noticeable red shift. Additionally, we found that dielectric confinement and quantum sound effects introduced significant changes, emphasizing the sensitivity to asymmetry and noncentrosymmetric behavior. Despite the limited experimental data available for BA_2SnI_4, our results are promising for optoelectronic applications, mainly because of the favorable exciton dissociation properties and larger absorption band. However, more research is required to fully realize the promise of the 2D RP BA_2SnI_4 perovskite, mainly about improving the PCE through device engineering and film quality for commercialization.

■ ASSOCIATED CONTENT

Data Availability Statement

The following Github repository: https://github.com/YonnatasBR/BA2SnI4-Optoelectronics, contains the calculation protocol and its step-by-step implementation.

Supporting Information

The Supporting Information is available free of charge at https://pubs.acs.org/doi/10.1021/acs.jpcc.5c01707.

Additional data and further details on the manuscript analysis (PDF)

■ AUTHOR INFORMATION

Corresponding Author

Maurício J. Piotrowski − *Department of Physics, Federal University of Pelotas, Pelotas, RS 96010-900, Brazil;* orcid.org/0000-0003-3477-4437; Email: mauriciomjp@gmail.com

Authors

J. F. Dalmedico − *Department of Physics, Federal University of Pelotas, Pelotas, RS 96010-900, Brazil*

D. N. Silveira − *Chemistry Department, Federal University of Paraná, Curitiba, PR 81531-980, Brazil;* orcid.org/0000-0001-6343-5560

Carlos Maciel O. Bastos − *Institute of Physics and International Center of Physics, University of Brasília, Brasília, DF 70919-970, Brazil*

C. R. C Rêgo − *Institute of Nanotechnology Hermann-von-Helmholtz-Platz, Karlsruhe Institute of Technology (KIT), 76021 Karlsruhe, Germany;* orcid.org/0000-0003-1861-2438

Alexandre Cavalheiro Dias − *Institute of Physics and International Center of Physics, University of Brasília, Brasília, DF 70919-970, Brazil*

D. Guedes-Sobrinho − *Chemistry Department, Federal University of Paraná, Curitiba, PR 81531-980, Brazil;* orcid.org/0000-0002-3313-2822

Complete contact information is available at: https://pubs.acs.org/10.1021/acs.jpcc.5c01707

Funding

The Article Processing Charge for the publication of this research was funded by the Coordenacao de Aperfeicoamento de Pessoal de Nivel Superior (CAPES), Brazil (ROR identifier: 00x0ma614).

Notes

The authors declare no competing financial interest.

■ ACKNOWLEDGMENTS

Authors thank the Rio Grande do Sul Research Foundation (FAPERGS, grant 24/2551−0001551−5), the Federal District Research Support Foundation (FAPDF, grants 00193−00001817/2023−43 and 00193-00002073/2023−84), the National Council for Scientific and Technological Development−CNPq (307345/2021−1, 408144/2022−0, 305174/2023−1, 444431/2024−1, 141176/2024−5, and 444069/2024−0), and the Coordination for Improvement of Higher Level Education−CAPES (finance Code 001) for the financial support. C. R. C. R. thanks the German Federal Ministry of

Education and Research (BMBF) for financial support of the project Innovation-Platform MaterialDigital (www.materialdigital.de) through project funding FKZ number: 13XP5094A. Part of this work was performed on the HoreKa supercomputer funded by the Ministry of Science, Research and the Arts Baden-Württemberg and by the Federal Ministry of Education and Research. The authors also thank the infrastructure provided to our computer cluster by the Department of Physics from the Federal University of Pelotas. This work also used resources of the "Centro Nacional de Processamento de Alto Desempenho em São Paulo" (CENAPAD-SP, UNICAMP/FINEP - MCTI), projects 897 and 570; of the "Centro Nacional de Supercomputação (CESUP-UFRGS)"; of the Lobo Carneiro HPC (NACAD) at the Federal University of Rio de Janeiro, from project 133; of the Ogun supercomputer of the CIMATEC SENAI at Salvador−BA; of the SDumont supercomputer in the Laboratório Nacional de Computação Científica (LNCC) at Petrópolis-RJ, as part of the "Sistema Nacional de Processamento de Alto Desempenho"−SINAPAD; and of the "Laboratório Central de Processamento de Alto Desempenho" (LCPAD), financed by FINEP through CT-INFRA/UFPR projects. A.C.D also acknowledge funding from PDPG-FAPDF-CAPES Centro-Oeste grant number 00193-00000867/2024−94.

REFERENCES

(1) Jung, M.-C.; Raga, S. R.; Qi, Y. Properties and solar cell applications of Pb-free perovskite films formed by vapor deposition. *RSC Adv.* **2016**, *6*, 2819−2825.
(2) Etgar, L. The merit of perovskite's dimensionality; can this replace the 3D halide perovskite? *Energy Environ. Sci.* **2018**, *11*, 234−242.
(3) Soe, C. M. M.; Nagabhushana, G. P.; Shivaramaiah, R.; Tsai, H.; Nie, W.; Blancon, J.-C.; Melkonyan, F.; Cao, D. H.; Traoré, B.; Pedesseau, L.; et al. Structural and thermodynamic limits of layer thickness in 2D halide perovskites. *Proc. Natl. Acad. Sci. U.S.A.* **2019**, *116*, 58−66.
(4) Blancon, J.-C.; Even, J.; Stoumpos, C. C.; Kanatzidis, M. G.; Mohite, A. D. Semiconductor physics of organic-inorganic 2D halide perovskites. *Nat. Nanotechnol.* **2020**, *15*, 969−985.
(5) Kumar, A.; Singh, S.; Mohammed, M. K.; Esmail Shalan, A. Effect of 2D perovskite layer and multivalent defect on the performance of 3D/2D bilayered perovskite solar cells through computational simulation studies. *Sol. Energy* **2021**, *223*, 193−201.
(6) Mitzi, D. B. Synthesis, Crystal Structure, and Optical and Thermal Properties of $(C_4H_9NH_3)_2MI_4$ (M = Ge, Sn, Pb). *Chem. Mater.* **1996**, *8*, 791−800.
(7) Soe, C. M. M.; Stoumpos, C. C.; Kepenekian, M.; Traoré, B.; Tsai, H.; Nie, W.; Wang, B.; Katan, C.; Seshadri, R.; Mohite, A. D.; et al. New Type of 2D Perovskites with Alternating Cations in the Interlayer Space, $(C(NH_2)_3)(CH_3NH_3)_nPb_nI_{3n+1}$: Structure, Properties, and Photovoltaic Performance. *J. Am. Chem. Soc.* **2017**, *139*, 16297−16309.
(8) Guedes-Sobrinho, D.; Guilhon, I.; Marques, M.; Teles, L. K. Relativistic DFT-1/2 Calculations Combined with a Statistical Approach for Electronic and Optical Properties of Mixed Metal Hybrid Perovskites. *J. Phys. Chem. Lett.* **2019**, *10*, 4245−4251.
(9) Rahil, M.; Ansari, R. M.; Prakash, C.; Islam, S. S.; Dixit, A.; Ahmad, S. Ruddlesden-Popper 2D perovskites of type $(C_6H_9C_2H_4NH_3)_2(CH_3NH_3)_{n-1}PbnI_{3n+1}$ (n = 1−4) for optoelectronic applications. *Sci. Rep.* **2022**, *12*, No. 2176.
(10) Guedes-Sobrinho, D.; Silveira, D. N.; de Araujo, L. O.; Dalmedico, J. F.; Wenzel, W.; Pramudya, Y.; Piotrowski, M. J.; Rêgo, C. R. C. Revealing the impact of organic spacers and cavity cations on quasi-2D perovskites via computational simulations. *Sci. Rep.* **2023**, *13*, No. 4446.
(11) Jeong, J.; Kim, M.; Seo, J.; Lu, H.; Ahlawat, P.; Mishra, A.; Yang, Y.; Hope, M. A.; Eickemeyer, F. T.; Kim, M.; et al. Pseudo-halide anion engineering for α-$FAPbI_3$ perovskite solar cells. *Nature* **2021**, *592*, 381−385.
(12) Wu, G.; Li, X.; Zhou, J.; Zhang, J.; Zhang, X.; Leng, X.; Wang, P.; Chen, M.; Zhang, D.; Zhao, K.; et al. Fine Multi-Phase Alignments in 2D Perovskite Solar Cells with Efficiency over 17% via Slow Post-Annealing. *Adv. Mater.* **2019**, *31*, No. 1903889.
(13) Masuko, K.; Shigematsu, M.; Hashiguchi, T.; Fujishima, D.; Kai, M.; Yoshimura, N.; Yamaguchi, T.; Ichihashi, Y.; Mishima, T.; Matsubara, N.; et al. Achievement of More Than 25% Conversion Efficiency With Crystalline Silicon Heterojunction Solar Cell. *IEEE J. Photovoltaics* **2014**, *4*, 1433−1435.
(14) Andreani, L. C.; Bozzola, A.; Kowalczewski, P.; Liscidini, M.; Redorici, L. Silicon solar cells: toward the efficiency limits. *Adv. Phys.:X* **2019**, *4*, No. 1548305.
(15) Jeon, N. J.; Na, H.; Jung, E. H.; Yang, T.-Y.; Lee, Y. G.; Kim, G.; Shin, H.-W.; Il Seok, S.; Lee, J.; Seo, J. A fluorene-terminated hole-transporting material for highly efficient and stable perovskite solar cells. *Nat. Energy* **2018**, *3*, 682−689.
(16) Liu, Z.; Lin, R.; Wei, M.; Yin, M.; Wu, P.; Li, M.; Li, L.; Wang, Y.; Chen, G.; Carnevali, V.; et al. All-perovskite tandem solar cells achieving > 29% efficiency with improved (100) orientation in wide-bandgap perovskites. *Nat. Mater.* **2025**, *24*, 252−259.
(17) Hoefler, S. F.; Trimmel, G.; Rath, T. Progress on lead-free metal halide perovskites for photovoltaic applications: a review. *Monatsh. Chem. - Chem. Mon.* **2017**, *148*, 795−826.
(18) Cao, J.; Yan, F. Recent progress in tin-based perovskite solar cells. *Energy Environ. Sci.* **2021**, *14*, 1286−1325.
(19) Noel, N. K.; Stranks, S. D.; Abate, A.; Wehrenfennig, C.; Guarnera, S.; Haghighirad, A.-A.; Sadhanala, A.; Eperon, G. E.; Pathak, S. K.; Johnston, M. B.; et al. Lead-free organic-inorganic tin halide perovskites for photovoltaic applications. *Energy Environ. Sci.* **2014**, *7*, 3061−3068.
(20) Li, X.; Guan, Y.; Li, X.; Fu, Y. Stereochemically Active Lone Pairs and Nonlinear Optical Properties of Two-Dimensional Multilayered Tin and Germanium Iodide Perovskites. *J. Am. Chem. Soc.* **2022**, *144*, 18030−18042.
(21) Zhang, X.; Ren, X.; Liu, B.; Munir, R.; Zhu, X.; Yang, D.; Li, J.; Liu, Y.; Smilgies, D.-M.; Li, R.; et al. Stable high efficiency two-dimensional perovskite solar cells via cesium doping. *Energy Environ. Sci.* **2017**, *10*, 2095−2102.
(22) Liang, C.; Gu, H.; Xia, Y.; Wang, Z.; Liu, X.; Xia, J.; Zuo, S.; Hu, Y.; Gao, X.; Hui, W.; et al. Two-dimensional Ruddlesden-Popper layered perovskite solar cells based on phase-pure thin films. *Nat. Energy* **2021**, *6*, 38−45.
(23) Cao, D. H.; Stoumpos, C. C.; Yokoyama, T.; Logsdon, J. L.; Song, T.-B.; Farha, O. K.; Wasielewski, M. R.; Hupp, J. T.; Kanatzidis, M. G. Thin films and solar cells based on semiconducting two-dimensional Ruddlesden-Popper $(CH_3(CH_2)_3NH_3)_2(CH_3NH_3)_{n-1}Sn_nI_{3n+1}$ perovskites. *ACS Energy Lett.* **2017**, *2*, 982−990.
(24) Konstantakou, M.; Stergiopoulos, T. A critical review on tin halide perovskite solar cells. *J. Mater. Chem. A* **2017**, *5*, 11518−11549.
(25) Kerner, R. A.; Christensen, E. D.; Harvey, S. P.; Messinger, J.; Habisreutinger, S. N.; Zhang, F.; Eperon, G. E.; Schelhas, L. T.; Zhu, K.; Berry, J. J.; et al. Analytical Evaluation of Lead Iodide Precursor Impurities Affecting Halide Perovskite Device Performance. *ACS Appl. Energy Mater.* **2023**, *6*, 295−301.
(26) Chen, Q.; De Marco, N.; Yang, Y. M.; Song, T.-B.; Chen, C.-C.; Zhao, H.; Hong, Z.; Zhou, H.; Yang, Y. Under the spotlight: The organic-inorganic hybrid halide perovskite for optoelectronic applications. *Nano Today* **2015**, *10*, 355−396.
(27) Zhou, H.; Chen, Q.; Li, G.; Luo, S.; Song, T.-b.; Duan, H.-S.; Hong, Z.; You, J.; Liu, Y.; Yang, Y. Interface engineering of highly efficient perovskite solar cells. *Science* **2014**, *345*, 542−546.

https://doi.org/10.1021/acs.jpcc.5c01707
J. Phys. Chem. C 2025, 129, 9646−9655

(28) Wang, Q.; Shao, Y.; Dong, Q.; Xiao, Z.; Yuan, Y.; Huang, J. Large fill-factor bilayer iodine perovskite solar cells fabricated by a low-temperature solution-process. *Energy Environ. Sci.* **2014**, *7*, 2359−2365.
(29) Abate, A. Perovskite Solar Cells Go Lead Free. *Joule* **2017**, *1*, 659−664.
(30) Liang, L.; Gao, P. Lead-Free Hybrid Perovskite Absorbers for Viable Application: Can We Eat the Cake and Have It too? *Adv. Sci.* **2018**, *5*, No. 1700331.
(31) Wu, G.; Liang, R.; Zhang, Z.; Ge, M.; Xing, G.; Sun, G. 2D Hybrid Halide Perovskites: Structure, Properties, and Applications in Solar Cells. *Small* **2021**, *17*, No. 2103514.
(32) Mitzi, D. B. Templating and structural engineering in organic-inorganic perovskites. *J. Chem. Soc., Dalton Trans.* **2001**, 1−12.
(33) Even, J.; Pedesseau, L.; Katan, C. Understanding Quantum Confinement of Charge Carriers in Layered 2D Hybrid Perovskites. *ChemPhysChem* **2014**, *15*, 3733−3741.
(34) Blancon, J.-C.; Stier, A. V.; Tsai, H.; Nie, W.; Stoumpos, C. C.; Traoré, B.; Pedesseau, L.; Kepenekian, M.; Katsutani, F.; Noe, G. T.; et al. Scaling law for excitons in 2D perovskite quantum wells. *Nat. Commun.* **2018**, *9*, No. 2254.
(35) Wu, G.; Liang, R.; Ge, M.; Sun, G.; Zhang, Y.; Xing, G. Surface Passivation Using 2D Perovskites toward Efficient and Stable Perovskite Solar Cells. *Adv. Mater.* **2022**, *34*, No. 2105635.
(36) Kang, J.; Wang, L.-W. Dynamic Disorder and Potential Fluctuation in Two-Dimensional Perovskite. The. *J. Phys. Chem. Lett.* **2017**, *8*, 3875−3880.
(37) Raja, A.; Waldecker, L.; Zipfel, J.; Cho, Y.; Brem, S.; Ziegler, J. D.; Kulig, M.; Taniguchi, T.; Watanabe, K.; Malic, E.; et al. Dielectric disorder in two-dimensional materials. *Nat. Nanotechnol.* **2019**, *14*, 832−837.
(38) Chen, C.; Kuai, Y.; Li, X.; Hao, J.; Li, L.; Liu, Y.; Ma, X.; Wu, L.; Lu, P. Impact of Halogen Substitution on the Electronic and Optical Properties of 2D Lead-Free Hybrid Perovskites. *J. Phys. Chem. C* **2021**, *125*, 15742−15750.
(39) Li, Y.; Zhou, H.; Xia, M.; Shen, H.; Wang, T.; Gao, H.; Sheng, X.; Han, Y.; Chen, Z.; Dou, L.; et al. Phase-pure 2D tin halide perovskite thin flakes for stable lasing. *Sci. Adv.* **2023**, *9*, No. eadh0517.
(40) Silveira, D. N.; Dias, A. C.; Araujo, L. O. d.; Queiroz, M. A.; Dalmedico, J. F.; Bastos, C. M. d. O.; Rêgo, C. R.; Piotrowski, M. J.; Guedes-Sobrinho, D. Excitonic properties and solar harvesting performance of $Cs_2ZnY_2X_2$ as quasi-2D mixed-halide perovskites. *J. Alloys Compd.* **2024**, *1007*, No. 176434.
(41) Marini, A.; Hogan, C.; Grüning, M.; Varsano, D. yambo: An ab initio tool for excited state calculations. *Comput. Phys. Commun.* **2009**, *180*, 1392−1403.
(42) Deslippe, J.; Samsonidze, G.; Strubbe, D. A.; Jain, M.; Cohen, M. L.; Louie, S. G. BerkeleyGW: A massively parallel computer package for the calculation of the quasiparticle and optical properties of materials and nanostructures. *Comput. Phys. Commun.* **2012**, *183*, 1269−1289.
(43) Leppert, L. Excitons in metal-halide perovskites from first-principles many-body perturbation theory. *J. Chem. Phys.* **2024**, *160*, No. 050902.
(44) Filip, M. R.; Qiu, D. Y.; Del Ben, M.; Neaton, J. B. Screening of Excitons by Organic Cations in Quasi-Two-Dimensional Organic-Inorganic Lead-Halide Perovskites. *Nano Lett.* **2022**, *22*, 4870−4878.
(45) Simbula, A.; Wu, L.; Pitzalis, F.; Pau, R.; Lai, S.; Liu, F.; Matta, S.; Marongiu, D.; Quochi, F.; Saba, M.; et al. Exciton dissociation in 2D layered metal-halide perovskites. *Nat. Commun.* **2023**, *14*, No. 4125.
(46) Guo, S.; Mihalyi-Koch, W.; Mao, Y.; Li, X.; Bu, K.; Hong, H.; Hautzinger, M. P.; Luo, H.; Wang, D.; Gu, J.; et al. Exciton engineering of 2D Ruddlesden-Popper perovskites by synergistically tuning the intra and interlayer structures. *Nat. Commun.* **2024**, *15*, No. 3001.
(47) Dias, A. C.; Silveira, J. F.; Qu, F. WanTiBEXOS: AWannier based Tight Binding code for electronic band structure, excitonic and optoelectronic properties of solids. *Comput. Phys. Commun.* **2023**, *285*, No. 108636.
(48) Dalmedico, J. F.; Silveira, D. N.; de Araujo, L. O..; Wenzel, W.; Rêgo, C. R. C..; Dias, A. C.; Guedes-Sobrinho, D.; Piotrowski, M. J. Tuning Electronic and Structural Properties of Lead-Free Metal Halide Perovskites: A Comparative Study of 2D Ruddlesden-Popper and 3D Compositions. *ChemPhysChem* **2024**, *25*, No. e202400118.
(49) Hohenberg, P.; Kohn, W. Inhomogeneous Electron Gas. *Phys. Rev.* **1964**, *136*, No. B864.
(50) Kohn, W.; Sham, L. J. Self-Consistent Equations Including Exchange and Correlation Effects. *Phys. Rev.* **1965**, *140*, No. A1133.
(51) Perdew, J. P.; Chevary, J. A.; Vosko, S. H.; Jackson, K. A.; Pederson, M. R.; Singh, D. J.; Fiolhais, C. Atoms, molecules, solids, and surfaces: Applications of the generalized gradient approximation for exchange and correlation. *Phys. Rev. B* **1992**, *46*, No. 6671.
(52) Perdew, J. P.; Burke, K.; Ernzerhof, M. Generalized Gradient Approximation Made Simple. *Phys. Rev. Lett.* **1996**, *77*, No. 3865.
(53) Kresse, G.; Furthmüller, J. Efficiency of ab-initio total energy calculations for metals and semiconductors using a plane-wave basis set. *Comput. Mater. Sci.* **1996**, *6*, 15−50.
(54) Kresse, G.; Furthmüller, J. Efficient iterative schemes for ab initio total-energy calculations using a plane-wave basis set. *Phys. Rev. B* **1996**, *54*, No. 11169.
(55) Kresse, G.; Joubert, D. From ultrasoft pseudopotentials to the projector augmented-wave method. *Phys. Rev. B* **1999**, *59*, No. 1758.
(56) Perdew, J. P. Density functional theory and the band gap problem. *Int. J. Quantum Chem.* **2009**, *28*, 497−523.
(57) Jones, R. O.; Gunnarsson, O. The density functional formalism, its applications and prospects. *Rev. Mod. Phys.* **1989**, *61*, 689−746.
(58) Perdew, J. P.; Yang, W.; Burke, K.; Yang, Z.; Gross, E. K. U.; Scheffler, M.; Scuseria, G. E.; Henderson, T. M.; Zhang, I. Y.; Ruzsinszky, A.; et al. Understanding band gaps of solids in generalized Kohn-Sham theory. *Proc. Natl. Acad. Sci. U.S.A.* **2017**, *114*, 2801−2806.
(59) Ferreira, L. G.; Marques, M.; Teles, L. K. Approximation to density functional theory for the calculation of band gaps of semiconductors. *Phys. Rev. B* **2008**, *78*, No. 125116.
(60) Ferreira, L. G.; Marques, M.; Teles, L. K. Slater half-occupation technique revisited: the LDA-1/2 and GGA-1/2 approaches for atomic ionization energies and band gaps in semiconductors. *AIP Adv.* **2011**, *1*, No. 032119.
(61) Grimme, S.; Hansen, A.; Brandenburg, J. G.; Bannwarth, C. Dispersion-Corrected Mean-Field Electronic Structure Methods. *Chem. Rev.* **2016**, *116*, 5105−5154.
(62) Rêgo, C. R. C.; Oliveira, L. N.; Tereshchuk, P.; Da Silva, J. L. F. Corrigendum: Comparative Study of van der Waals Corrections to the Bulk Properties of Graphite (2015 J. Phys.: Condens. Matter 27 415502). *J. Phys.: Condens. Matter* **2016**, *28*, No. 129501.
(63) Rêgo, C. R. C.; Oliveira, L. N.; Tereshchuk, P.; Da Silva, J. L. F. Comparative Study of van der Waals Corrections to the Bulk Properties of Graphite. *J. Phys.: Condens. Matter* **2015**, *27*, No. 415502.
(64) de Araujo, L. O.; Sabino, F. P.; Rêgo, C. R. C.; Guedes-Sobrinho, D. Bulk Rashba Effect Splitting and Suppression in Polymorphs of Metal Iodine Perovskites. *J. Phys. Chem. Lett.* **2021**, *12*, 7245−7251.
(65) Koelling, D. D.; Harmon, B. N. A technique for relativistic spin-polarised calculations. *J. Phys. C: Solid State Phys.* **1977**, *10*, 3107−3114.
(66) Takeda, T. The scalar relativistic approximation. *Z. Phys. B:Condens. Matter Quanta* **1978**, *32*, 43−48.
(67) Blöchl, P. E. Projector augmented-wave method. *Phys. Rev. B* **1994**, *50*, No. 17953.
(68) Mostofi, A. A.; Yates, J. R.; Lee, Y.-S.; Souza, I.; Vanderbilt, D.; Marzari, N. Wannier90: A tool for obtaining maximally-localised Wannier functions. *Comput. Phys. Commun.* **2008**, *178*, 685−699.
(69) Salpeter, E. E.; Bethe, H. A. A Relativistic Equation for Bound-State Problems. *Phys. Rev.* **1951**, *84*, No. 1232.

https://doi.org/10.1021/acs.jpcc.5c01707
J. Phys. Chem. C 2025, 129, 9646−9655

(70) ASTM-G173−03 Standard Tables for Reference Solar Spectral Irradiances: Direct Normal and Hemispherical on 37° Tilted Surface. 2012 .
(71) Rêgo, C. R. C.; Schaarschmidt, J.; Schlöder, T.; Penaloza-Amion, M.; Bag, S.; Neumann, T.; Strunk, T.; Wenzel, W. SimStack: An Intuitive Workflow Framework. *Front. Mater.* **2022**, *9*, No. 877597.
(72) Mieller, B.; Valavi, M.; Rêgo, C. R. C. An Automatized Simulation Workflow for Powder Pressing Simulations Using SimStack. *Adv. Eng. Mater.* **2024**, No. 2400872.
(73) Rêgo, C. R. C.; Wenzel, W.; Piotrowski, M. J.; Dias, A. C.; de Oliveira Bastos, C. M.; de Araujo, L. O.; Guedes-Sobrinho, D. Digital workflow optimization of van der Waals methods for improved halide perovskite solar materials. *Digital Discovery* **2025**, *4*, 927−942.
(74) Da Silva, G. R.; Felix, J. P. C.; Rêgo, C. R. C.; Dias, A. C.; Bastos, C. M. d. O.; Piotrowski, M. J.; Guedes-Sobrinho, D. Workflow-driven catalytic modulation from single-atom catalysts to Au-alloy clusters on graphene. *Sci. Rep.* **2025**, *15*, No. 1939.
(75) Schaarschmidt, J.; Yuan, J.; Strunk, T.; Kondov, I.; Huber, S. P.; Pizzi, G.; Kahle, L.; Bölle, F. T.; Castelli, I. E.; Vegge, T.; et al. Workflow Engineering in Materials Design within the BATTERY 2030+ Project. *Adv. Energy Mater.* **2022**, *12*, No. 2102638.
(76) Soleymanibrojeni, M.; Rego, C. R. C.; Esmaeilpour, M.; Wenzel, W. An active learning approach to model solid-electrolyte interphase formation in Li-ion batteries. *J. Mater. Chem. A* **2024**, *12*, 2249−2266.
(77) de Araujo, L. O.; Rêgo, C. R. C.; Wenzel, W.; Piotrowski, M. J.; Dias, A. C.; Guedes-Sobrinho, D. Automated workflow for analyzing thermodynamic stability in polymorphic perovskite alloys. *npj Comput. Mater.* **2024**, *10*, No. 146.
(78) Bekemeier, S.; Rêgo, C. R. C.; Mai, H. L.; Saikia, U.; Waseda, O.; Apel, M.; Arendt, F.; Aschemann, A.; Bayerlein, B.; Courant, R.; et al. Advancing Digital Transformation in Material Science: The Role of Workflows Within the MaterialDigital Initiative. *Adv. Eng. Mater.* **2025**, *27*, No. 2402149.
(79) Hansen, K. R.; McClure, C. E.; Colton, J. S.; Whittaker-Brooks, L. Franz-Keldysh and Stark Effects in Two-Dimensional Metal Halide Perovskites. *PRX Energy* **2022**, *1*, No. 013001.
(80) De Angelis, F. The Prospect of Lead-Free Perovskite Photovoltaics. *ACS Energy Lett.* **2021**, *6*, 1586−1587.
(81) Hansen, K. R.; McClure, C. E.; Powell, D.; Hsieh, H.-C.; Flannery, L.; Garden, K.; Miller, E. J.; King, D. J.; Sainio, S.; Nordlund, D.; et al. Low Exciton Binding Energies and Localized Exciton-Polaron States in 2D Tin Halide Perovskites. *Adv. Opt. Mater.* **2022**, *10*, No. 2102698.
(82) Ma, L.; Ju, M.-G.; Dai, J.; Zeng, X. C. Tin and germanium based two-dimensional Ruddlesden-Popper hybrid perovskites for potential lead-free photovoltaic and photoelectronic applications. *Nanoscale* **2018**, *10*, 11314−11319.
(83) Ma, L.; Dai, J.; Zeng, X. C. Two-Dimensional Single-Layer Organic-Inorganic Hybrid Perovskite Semiconductors. *Adv. Energy Mater.* **2017**, *7*, No. 1601731.
(84) Azizman, M. S. A.; Azhari, A. W.; Halin, D. S. C.; Ibrahim, N.; Sepeai, S.; Ludin, N. A.; Nor, M. N. M.; Ho, L. N. Progress in tin-germanium perovskite solar cells: A review. *Synth. Met.* **2023**, *299*, No. 117475.
(85) Wang, D.; Liang, P.; Dong, Y.; Shu, H.; Liu, Z. Electronic and optical properties of layered Ruddlesden Popper hybrid $X_2(MA)_{n-1}Sn_nI_{3n+1}$ perovskite insight by first principles. *J. Phys. Chem. Solids* **2020**, *144*, No. 109510.
(86) Hong, X.; Ishihara, T.; Nurmikko, A. V. Dielectric confinement effect on excitons in PbI-based layered semiconductors. *Phys. Rev. B* **1992**, *45*, No. 6961.
(87) Tanaka, K.; Kondo, T. Bandgap and exciton binding energies in lead-iodide-based natural quantum-well crystals. *Sci. Technol. Adv. Mater.* **2003**, *4*, 599−604.
(88) Tanaka, K.; Takahashi, T.; Kondo, T.; Umebayashi, T.; Asai, K.; Ema, K. Image charge effect on two-dimensional excitons in an inorganic-organic quantum-well crystal. *Phys. Rev. B* **2005**, *71*, No. 045312.
(89) Traore, B.; Pedesseau, L.; Assam, L.; Che, X.; Blancon, J.-C.; Tsai, H.; Nie, W.; Stoumpos, C. C.; Kanatzidis, M. G.; Tretiak, S.; et al. Composite Nature of Layered Hybrid Perovskites: Assessment on Quantum and Dielectric Confinements and Band Alignment. *ACS Nano* **2018**, *12*, 3321−3332.
(90) Passarelli, J. V.; Mauck, C. M.; Winslow, S. W.; Perkinson, C. F.; Bard, J. C.; Sai, H.; Williams, K. W.; Narayanan, A.; Fairfield, D. J.; Hendricks, M. P.; et al. Tunable exciton binding energy in 2D hybrid layered perovskites through donor-acceptor interactions within the organic layer. *Nat. Chem.* **2020**, *12*, 672−682.
(91) Li, G.; Su, Z.; Li, M.; Yang, F.; Aldamasy, M. H.; Pascual, J.; Yang, F.; Liu, H.; Zuo, W.; Di Girolamo, D.; et al. Ionic liquid stabilizing high-efficiency tin Halide perovskite solar cells. *Adv. Energy Mater.* **2021**, *11*, No. 2101539.
(92) Cho, S.; Pandey, P.; Yoon, S.; Ryu, J.; Lee, D.-G.; Shen, Q.; Hayase, S.; Song, H.; Choi, H.; Ahn, H.; et al. Anchoring self-assembled monolayer at perovskite/hole collector interface for wide bandgap Sn-based solar cells with a record efficiency over 12%. *Surf. Interfaces* **2023**, *42*, No. 103478.
(93) Jiang, Y.; Cui, M.; Li, S.; Sun, C.; Huang, Y.; Wei, J.; Zhang, L.; Lv, M.; Qin, C.; Liu, Y.; Yuan, M. Reducing the impact of Auger recombination in quasi-2D perovskite light-emitting diodes. *Nat. Commun.* **2021**, *12*, No. 336.
(94) Gong, X.; Voznyy, O.; Jain, A.; Liu, W.; Sabatini, R.; Piontkowski, Z.; Walters, G.; Bappi, G.; Nokhrin, S.; Bushuyev, O.; et al. Electron−phonon interaction in efficient perovskite blue emitters. *Nat. Mater.* **2018**, *17*, 550−556.
(95) Gong, J.; Hao, M.; Zhang, Y.; Liu, M.; Zhou, Y. Layered 2D Halide perovskites beyond the Ruddlesden-Popper phase: Tailored interlayer chemistries for high-performance solar cells. *Angew. Chem., Int. Ed.* **2022**, *61*, No. e202112022.
(96) Dong, J.; Shao, S.; Kahmann, S.; Rommens, A. J.; Hermida-Merino, D.; ten Brink, G. H.; Loi, M. A.; Portale, G. Mechanism of Crystal Formation in Ruddlesden-Popper Sn-Based Perovskites. *Adv. Funct. Mater.* **2020**, *30*, No. 2001294.
(97) Jena, A. K.; Kulkarni, A.; Miyasaka, T. Halide perovskite photovoltaics: Background, status, and future prospects. *Chem. Rev.* **2019**, *119*, 3036−3103.
(98) Hao, F.; Stoumpos, C. C.; Cao, D. H.; Chang, R. P. H.; Kanatzidis, M. G. Lead-free solid-state organic-inorganic halide perovskite solar cells. *Nat. Photonics* **2014**, *8*, 489−494.

https://doi.org/10.1021/acs.jpcc.5c01707
J. Phys. Chem. C 2025, 129, 9646−9655